

RX J1856 – 3754: EVIDENCE FOR A STIFF EOS

TIMOTHY M. BRAJE AND ROGER W. ROMANI
 Physics Department, Stanford University, Stanford, CA 94305
 timb@astro.stanford.edu, rwr@astro.stanford.edu
ApJ in press.

ABSTRACT

We have examined the soft X-ray plus optical/UV spectrum of the nearby isolated neutron star RX J1856 – 3754, comparing with detailed models of a thermally emitting surface. Like previous investigators, we find the spectrum is best fit by a two-temperature blackbody model. In addition, our simulations constrain the allowed viewing geometry from the observed pulse fraction upper limits. These simulations show that RX J1856 – 3754 is very likely to be a normal young pulsar, with the non-thermal radio beam missing Earth’s line of sight. The SED limits on the model parameter space put a strong constraint on the star’s M/R . At the measured parallax distance, the allowed range for $M_{\text{NS}} = 1.5M_{\odot}$ is $R_{\text{NS}} = 13.7 \pm 0.6$ km. Under this interpretation, the EOS is relatively stiff near nuclear density and the ‘Quark Star’ EOS posited in some previous studies is strongly excluded. The data also constrain the surface T distribution over the polar cap.

Subject headings: stars: neutron, equation of state

1. INTRODUCTION

RX J1856 – 3754, discovered by Walter, Wolk, & Neuhäuser (1996), is the nearest and brightest known neutron star not showing emission dominated by non-thermal magnetospheric processes. As such it offers a unique opportunity to study the bare thermal surface emission. Measurements of the spectrum can probe the neutron star mass (M_{NS}) and radius (R_{NS}), constraining the high density equation of state (EOS). Since the discovery, there have been several intensive observing campaigns covering the optical-UV (*HST*) and most recently the detailed soft X-ray spectrum (*CXO*). An initial 50ks Low-Energy Transmission Grating (LETG) spectrum showed a broad band spectrum remarkably consistent with a simple blackbody (Burwitz *et al.* 2001), although hints of spectral features were suggested (van Kerkwijk 2002). A deeper observation using 450 ks of Director’s Discretionary Time (DDT) was made. This unique data set has been the subject of prompt study; several authors show that lines in the spectrum are undetectable, while pulse searches have placed stringent limits on the observed soft X-ray pulse fraction (Ransom, Gaensler, & Slane 2002; Drake *et al.* 2002). These data have been variously interpreted, including the widely reported speculation (based on the X-ray spectrum alone) that RX J1856 – 3754 might be a bare quark star (esp. Drake *et al.* 2002).

Despite the very stringent constraints placed on the X-ray pulse fraction, ($< 4.5\%$ at 99% confidence, including a \dot{P} search Ransom, Gaensler, & Slane 2002), there is strong evidence that RX J1856 – 3754 is a rotation-powered pulsar. van Kerkwijk & Kulkarni (2001b) discovered an H α nebula surrounding the neutron star, concluding that it could be best interpreted as a bow-shock nebula powered by a relativistic wind of e^{\pm} generated by pulsar spindown. The bow shock geometry then provides an estimate of the spindown power $\dot{E} = I\Omega\dot{\Omega} = 8 \times 10^{32}$ erg/s d_{140}^3 (van Kerkwijk & Kulkarni 2001b). Adopting magnetic dipole braking at constant B , this gives $\dot{E} = 10^{34}(B_{12}\tau_6)^{-2}$ erg/s

for a surface dipole field $10^{12}B_{12}$ G and characteristic age $10^6\tau_6$ y, suggesting $B_{12}\tau_6 \sim 3$.

A critical parameter in the discussion of this source is the distance, which has been the subject of some controversy. Initial estimates from *HST* astrometry gave a parallax distance of 61 pc (Walter 2001). Kaplan, van Kerkwijk, & Anderson (2002), however re-analyzed these data, deriving $d = 143$ pc. A fourth *HST* observation appears to have resolved this discrepancy, giving an overall measurement of $d = 117 \pm 12$ pc (Walter & Lattimer 2002); we adopt this value.

2. SPECTRAL FITS

For some time now, it has been clear that the broad band spectrum of RX J1856 – 3754 from *HST*, *ROSAT*, and *EUVE* data (for a detailed discussion, see Pons *et al.* 2002) is inconsistent with a light element (\sim Kramer’s law opacity) H or He atmospheres. H models, for example, overpredict the optical/X-ray flux ratio by a factor ~ 100 (Pavlov *et al.* 1996). Blackbody, heavy element or composite models gave acceptable fits. To produce such \sim Planckian spectra, one must have nearly isothermal conditions at optical depth $\tau_{\nu} \approx 1$ across the observed band. One possibility is that the surface is in a solid or liquid state, precluding large temperature gradients through the photosphere. Theoretical studies to date, while limited, suggest that this is not the case unless H is present and $B > 10^{13}$ G (Lai & Salpeter 1997). In an atmosphere, the easiest way to form the spectrum in a small depth range is to invoke a rich line spectrum; thus, at first sight, blackbody-like spectra should require a high spectral density of opacity features (lines and edges). This led to the expectation that the blackbody-like spectrum of RX J1856 – 3754 would show many spectral features when examined with good S/N LETG spectra. Unfortunately, the initial 50 ks exposure already showed that the line features were substantially weaker than expected in a simple low- B single temperature atmosphere model dominated by heavy elements. The new DDT exposure only enhances this conclu-

sion, placing very strong limits (typical equivalent width $\lesssim 0.02\text{\AA}$ Drake *et al.* 2002) on spectral features.

We will be concerned with the quality of statistical fits to various atmosphere models. It is important to note here that blackbody spectral fits to the *CXO* RX J1856 – 3754 LETG data are, contrary to early reports, *not* statistically perfect fits to a simple Planck spectrum. This conclusion was drawn from fits to basic CIAO extractions, which appreciably underbin the spectrum. Instead we find that at a more modest binning (equally spaced $\sim 0.7\text{\AA}$ bins) we obtain $\chi^2/\text{DOF}=1.6$. As the bin size is increased, the χ^2/DOF grows to ~ 4.8 , until the number of degrees of freedom becomes small. This is a clear signature of spectral departures on resolved energy scales, and with appropriate binning one indeed finds systematic, grouped residuals to the Planck function fit at the $\sim 10\%$ level. We believe that these represent the limit of accuracy in calibration of the response matrix, as the broad band spectral shape is an excellent fit to the Planck function. Drake *et al.* (2002) have reached similar conclusions. Recognizing that very subtle departures from a pure blackbody may be present in these data, we adopt the conservative assumption that these departures are fully accounted for by response matrix systematics.

To accommodate an extended atmosphere, one must suppress the spectral features. One possibility is that external heat sources (such as precipitating magnetospheric e^\pm) drive the atmosphere towards isothermality. Sample atmospheres showing this effect have been computed in Gänsicke, Braje, & Romani (2002). A second possibility is that the line energies for a given species vary strongly across the neutron star surface. For normal pulsar fields, $B \sim 10^{12}$ G or higher, the strong dependence of the transition energies on the local B (*eg.* Rajagopal, Romani, & Miller 1997; Pavlov *et al.* 1995), coupled with substantial $\geq 2\times$ variation of B across the surface, even for the simplest dipole models, ensures that such ‘magnetic smearing’ will strongly suppress the phase-averaged line width (Romani, *in prep.*). We discuss briefly here a third possibility, that the lines experience variable shifts as the pulsar rotates due to Doppler and other dynamic effects. Again, the phase-averaged spectrum observed for RXJ1856 – 3754 would be expected to show broadened and blended lines, driving the spectrum towards a Planck curve.

If, as is required for a normal neutron star, the soft X-ray emission of RX J1856 – 3754 is dominated by hot polar caps, the rotation of these past the line of sight produces phase dependent Doppler shifts (Braje, Romani, & Rauch 2000). These are only significant for $v_{surf} \sim 2\pi R_{NS}/P_{NS} \rightarrow c$, *i.e.* $P_{NS} \lesssim$ a few ms. Such small P_{NS} are not excluded, since the HRC-S wiring error limits arrival time accuracy and precludes sensitive searches for $P_{NS} \lesssim 10$ ms. Moreover, the \dot{E} from the bow shock stand-off gives $P_{NS} = 4.6(B/10^8 \text{ G})^{1/2}$ ms, so a low field star, having a non-magnetic atmosphere would have a \sim ms spin period.

For a concrete example, we assume $M_{NS} = 1.4M_\odot$, $R_{NS} = 10$ km, and $P_{NS} = 1.5$ ms (allowed, as the existence of *PSR* 1937 + 21 shows). We have tried both solar abundance and iron model atmospheres, tested a range of magnetic inclinations α , and computed phase averaged spectra using an extension of the Monte Carlo simulation

code described in Braje, Romani, & Rauch (2000). We then tested these models, fitting the most recent *CXO* data, allowing the temperature, observer viewing angle ζ , and interstellar absorption n_H to vary. The large L and M shell edges in the iron models ensure that these are always poor fits. The solar abundance atmospheres have a much richer line structure which is more easily blurred into a pseudo-continuum. In Figure 1, we display the solar abundance millisecond pulsar model, overlaid on the *CXO* data. For comparison the best fit non-rotating model is shown in the upper panel. Doppler boosting produces a qualitatively acceptable fit below ~ 0.5 keV, but the simple blackbody remains statistically an appreciably better model ($\chi^2/\text{DOF}=1.6$ *vs.* 3.7 for the binning chosen). We must conclude that a simple blackbody fit remains the best available, although not yet physically explained. Planck emission from a physical neutron star can be compared with the data to obtain significant constraints on the neutron star parameters; we pursue this in the remainder of the paper.

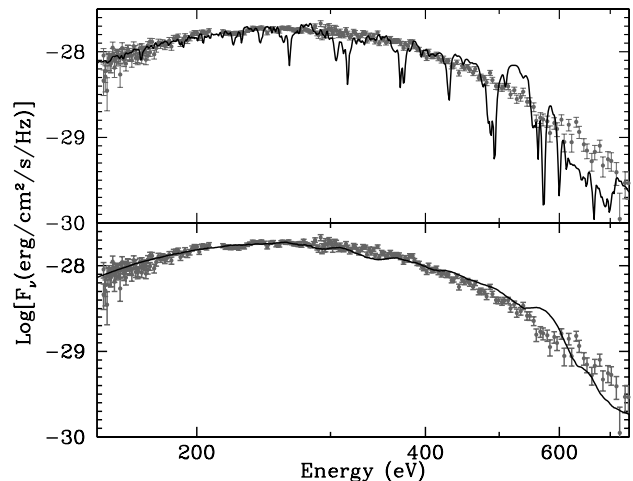


FIG. 1.— *Top*: Best fit solar abundance model with no Doppler shifts. *Bottom*: Best fit solar abundance model with Doppler shifts for a $P_{NS} = 1.5$ ms, $R_{NS} = 10$ km pulsar.

3. TWO TEMPERATURE BLACKBODY FITS

A blackbody fit to the *CXO* data alone results in a temperature of $T_\infty \sim 61$ eV with very small statistical uncertainty (Drake *et al.* 2002, and our own analysis). We find, as also reported by Drake *et al.* (2002), that systematics (likely in the effective area, as noted above) provide the dominant error. Drake *et al.* (2002) quote 61.2 ± 1.0 eV. Taken at face value this T_∞ with the parallax distance gives a radius as measured at infinity of $R_\infty = (1+z)R_{NS} = 3.8 - 8.2$ km. If interpreted as the full star radius, this demands exotic equations of state (*i.e.* quark stars). Of course, this is only a lower limit to the stellar radius. The optical/UV data points, which closely follow a Rayleigh-Jeans spectrum (*eg.* Pons *et al.* 2002; van Kerkwijk & Kulkarni 2001a), are most easily interpreted as a second cooler Planck spectrum representing flux from the full surface. This has been previously recognized, but Drake *et al.* (2002) argue against this interpretation, citing the absence of the X-ray pulse expected from such a hot polar cap/cool surface combination. We have

addressed this concern quantitatively, computing detailed light curves and spectra.

3.1. Analytic Two-Temperature Models

A simple analytic two-temperature blackbody fit delineates the basic model parameters. For a range of effective (cold surface) radii, we fit T_{hot} , T_{cold} , the hot area, and the absorption column density. In Figure 2, we plot the minimum χ^2 as a function of cold radius. The optical-UV data points fix $R_{\text{NS}}^2 T_{\text{cold}}$. The fit becomes poor when T_{cold} starts to allow significant Wien peak contribution to the *CXO* X-ray band; this sets the minimum stellar radius. Formally, there is a maximum acceptable radius beyond which low T_{cold} predicts Wien peak curvature inconsistent with the \sim Rayleigh-Jeans UV data points.

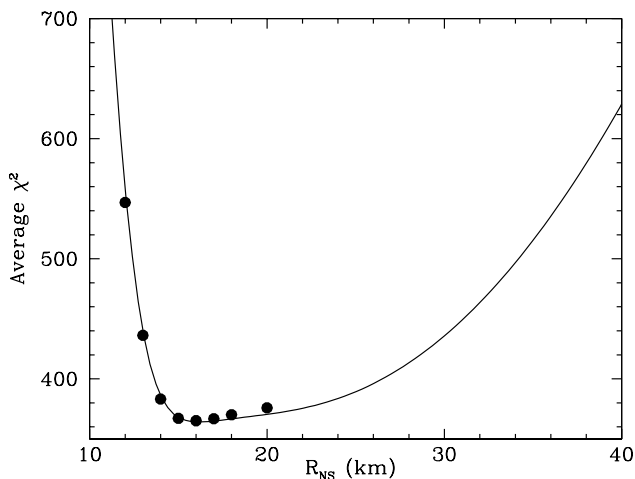


FIG. 2.— Solid line: χ^2 (257 DOF) as a function of cold sphere radius. Points: χ^2 values from the polar-cap model fits.

3.2. More Realistic Two-Temperature Models

In addition to the phase averaged spectrum, we have a limit on the *CXO*-band pulse fraction. A more realistic model is required to address the detailed spectrum and pulsations. We adopt a two-temperature model with two opposing hot spots (polar caps) at T_{hot} and the remainder of the surface at T_{cold} . The caps' orientation (α and ζ) are free parameters. We radiate from these surfaces, tracing the photons to infinity to form phase resolved spectra and light curves. For details of these Monte-Carlo sums see Braje, Romani, & Rauch (2000).

The analytic model results allow some useful simplifications. Since T_{hot} is virtually constant over the full acceptable R_{NS} range, we fix this value in exploring the rest of the parameter space. Further, the X-ray flux amplitude allows an initial estimate of the cap half angle Δ (which depends on α and ζ) that ensures that the pulse formation is accurate and results in quick convergence to the true minimum.

The fit parameters of interest are R_{NS} , Δ , T_{cold} , ζ , α , and n_{H} . To explore the sensitivity to several parameters, we have computed a model grid. We calculate all models for $\alpha = 5^\circ$ to $\alpha = 90^\circ$ in five degree steps; $\zeta = 0^\circ$ to $\zeta = 90^\circ$ in five degree steps; and $R_{\text{NS}} = 12$ km to $R_{\text{NS}} = 20$ km in one kilometer steps. While not strictly a fit

parameter, we also vary the stellar mass M_{NS} . The quality of the spectral fit turns out to be quite insensitive to the choice of α and ζ . In Figure 3, we display a typical spectrum for a model with $M_{\text{NS}} = 1.4M_{\odot}$, $R_{\text{NS}} \gtrsim 14$ km. As the radius becomes smaller, the optical-UV flux is under-predicted and the fit becomes unacceptable.

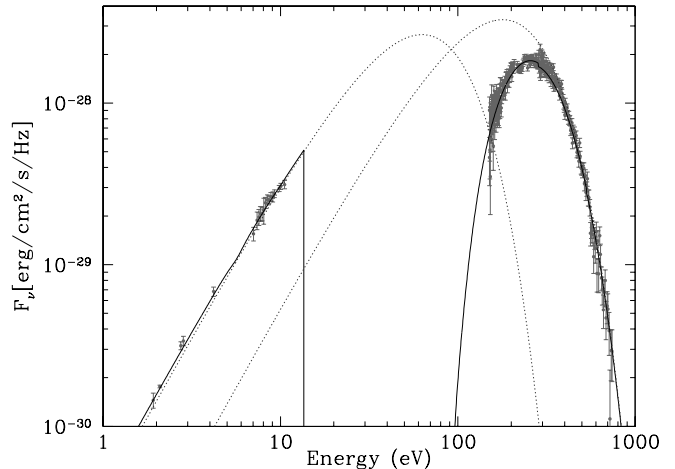


FIG. 3.— Broad band spectral fit to RXJ1856–3754. Optical/UV data points are drawn from van Kerkwijk & Kulkarni (2001a) and Pons *et al.* (2002). The dotted lines show the unabsorbed hot and cold blackbody components.

For each α and ζ we compute χ^2 as a function of R_{NS} . The average over angles is shown by the points in Figure 2. Note that the minimum value is not at $\chi^2_{\nu} = 1$, a consequence of the aforementioned systematic errors. This means that the errors are not Poisson distributed according to the bin counts. To establish confidence levels (CL), we must Monte Carlo according to the observed error distribution. We have computed the χ^2 distribution about the best fit model for each (α, ζ) combination, obtaining a histogram of χ^2 values. These were almost completely insensitive to the angles, so we combined all the χ^2 distributions to obtain confidence levels to the χ^2 increases associated with variations in R_{NS} . Examinations of the differences between the different angles and between independent Monte Carlo runs show that the estimates of 90% and 99% confidence level limits on the radius are uncertain by no more than ± 0.5 km from systematic and computational errors in this procedure.

3.3. Cap Shape Constraints

One might question whether a simple, circular uniform T_{hot} polar cap is merely an adequate approximation to the data. We have fit some alternative surface temperature distributions $T(\eta)$, where η is the magnetic colatitude, comparing with the best fit circular cap which had $kT_{\text{hot}} = 62.8$ eV, $\Delta = 21^\circ$. The best fit Gaussian $T(\eta)$ had a peak temperature of $kT_{\text{hot}} = 74.8$ eV and width $\sigma = 19^\circ$, but showed an increase of $\chi^2 \approx 80$ over the simple cap model, sufficient to exclude at the $\sim 99\%$ CL. Adding a simple linear T_{hot} to T_{cold} ramp to a uniform cap makes no discernible difference until the ramp width is twice that of the cap. At this point the best fit model has a cap with $kT_{\text{hot}} = 69$ eV and $\Delta \approx 12^\circ$, but the model is excluded at the $\sim 90\%$ CL. Finally, we fit both a simple $T_{\text{hot}} \propto \cos(\eta)$

model and the surface $T(\eta)$ distribution of Greenstein & Hartke (1983) which is motivated by magnetic anisotropy in the thermal conductivity. Both were excluded by the *CXO* data at very high confidence. All fits were at $1.4M_{\odot}$, best fit stellar radii and (α, ζ) chosen so that the pulse fraction is $\lesssim 5\%$ for the default cap model.

Evidently, the *CXO* data require a quite uniform distribution of the high temperature excess, and suggests that it is induced by exterior heating rather than interior conductivity. This cap size is substantially larger than the $\Delta \sim 3^{\circ}(100 \text{ ms}/P_{\text{NS}})^{1/2}$ expected for a dipole surface cap, unless the period is very small. Higher magnetic multipoles would generally have even smaller open zone caps. The large, uniformly heated area is puzzling in the context of pulsar surface acceleration models, but might be most easily accommodated in the more modern pictures of a GR-induced potential that is relatively uniform across the polar cap and forms a pair formation front at relatively high altitudes (Harding & Muslimov 1998). Perhaps a more plausible interpretation invokes a high-altitude acceleration zone, with the inward-directed γ -rays pair converting in the closed zone above the polar cap (Wang *et al.* 1998), which should give a \sim large zone of uniform surface heating.

4. PULSE FRACTION CONSTRAINTS

We have seen that the spectral fits are quite insensitive to the cap viewing angles. They place a firm minimum on the allowed R_{NS} but allow radii that are implausibly large. However, the observed pulse fraction depends strongly on viewing geometry and, through gravitational focusing, the value of $M_{\text{NS}}/R_{\text{NS}}$. In general, we expect a strong X-ray pulse when the magnetic axis passes close to Earth's line-of-sight (small $|\alpha - \zeta|$). Of course, for an aligned rotator $\alpha \approx 0$ the pulse can be very small and for $\alpha \approx \pi/2$ there is an appreciable region where the pulse is weak as viewed from Earth. We have examined the *CXO*-band pulse profile of our model grid to find the allowed region of (α, ζ) parameter space in which the model pulse fraction is weaker than that observed ($\lesssim 4.5\%$); this is shown in the inset of Figure 4.

This exercise is repeated for each $M_{\text{NS}}, R_{\text{NS}}$; the allowed phase space is larger for small $R_{\text{NS}}/M_{\text{NS}}$ as gravitational bending dilutes the observed pulse. By demanding a certain minimum probability that a pulse fraction as low as that observed is seen at Earth, we obtain a *maximum* acceptable radius for the neutron star. One important additional constraint can be invoked. The non-detection of this neutron star in the radio band (Brazier & Johnston 1999) puts a very strong bound on pulsar emission directed towards Earth. Assuming that this is a normal radio pulsar (consistent with \dot{E} inferred from the bow shock), we must conclude *a priori* (independent of the X-ray data) that our line of sight lies outside of the pulsar radio beam and that $|\alpha - \zeta|$ is not small. The region excluded depends on the size of the radio beam (Θ_{rad}), which in turn depends on the spin period. A typical estimate is (*eg.* Rankin 1993)

$$\Theta_{\text{rad}} = 5.8^{\circ}(P_{\text{NS}}/1\text{s})^{-1/2} \quad (1)$$

at the radio frequency $\nu = 1 \text{ GHz}$. With $P_{\text{NS}} = 0.3 \text{ s}$, this gives $\Theta_{\text{rad}} \sim 10.6^{\circ}$. Radio limits on RX J1856 – 3754 are strong at even lower ν where radius-to-frequency mapping

produces larger Θ_{rad} , and for this nearby object, the radio luminosity constraints are so severe that we are unlikely to intersect even the faint fringe of the radio beam. Both effects argue for Θ_{rad} larger than that above. Accordingly, in the Figure 4 inset we show by diagonal lines the regions near $\alpha = \zeta$ excluded by the lack of radio detection for $1\times$ and $2\times$ this fiducial beam size. Shorter periods allow an *a priori* exclusion of even more phase space. The point is that from the lack of radio detection we should have *expected* a low X-ray pulse fraction. The probability for obtaining pulses as weak as observed is then set by the fraction of the remaining allowed solid angle. These fractions are plotted in Figure 4 with and without the radio prior. The allowed radius range depends on mass and in Table 1, we give the 90% and 99% CL upper bound on the neutron star radius for these priors and several neutron star masses.

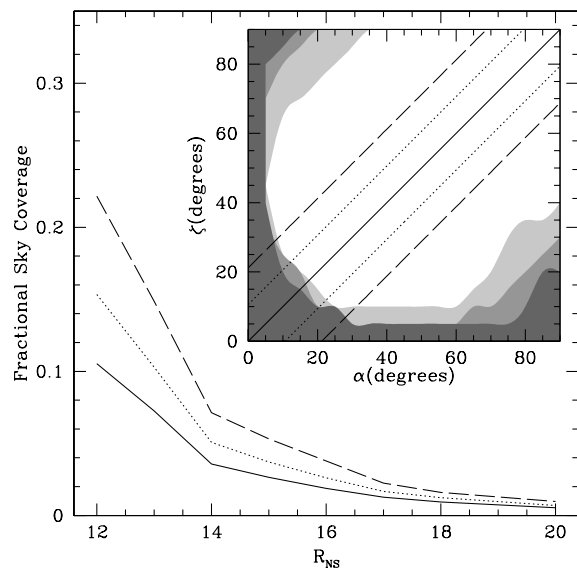


FIG. 4.— Fraction of the sky allowed by pulse fraction constraints as a function of stellar radius. The solid line assumes no priors; the dotted line for a prior $1 \times \Theta_{\text{rad}} = 10.6^{\circ}$; and the dashed line for $2 \times \Theta_{\text{rad}}$. The inset shows the allowed (α, ζ) parameter space shaded in light, medium, and dark gray for 12, 14, 16 km, respectively at $M_{\text{NS}} = 1.4M_{\odot}$. The lines in the inset depict the parameter space excluded by radio prior.

5. EQUATION OF STATE CONSTRAINT

We see that the X-ray/optical data, using the spectral and pulse fraction arguments, give a range of allowed stellar radii for each mass. Strictly speaking, the minimum and maximum radius CL have somewhat different interpretations, but it is interesting to place these bounds in the $M_{\text{NS}} - R_{\text{NS}}$ plane to compare with the predictions of various EOS.

In Figure 5, we show the combined constraints, assuming $\Theta_{\text{rad}} = 21.2^{\circ}$. The spectral radius lower bounds at 90% and 99% CL approximate curves of constant $M_{\text{NS}}/R_{\text{NS}}$. The pulse fraction upper bounds (90%, 95%) rapidly drive one to small radii at low masses. For $M_{\text{NS}} \lesssim 1.3M_{\odot}$ no simultaneous solutions are allowed consistent with the 90% bounds. At $M_{\text{NS}} = 1.5M_{\odot}$ the allowed range from the fit is quite small, $R_{\text{NS}} = 13.7 \pm 0.6 \text{ km}$. The additional uncertainty in the distance actually dominates the errors

(arrowed bar).

For comparison, several EOS curves (after Lattimer & Prakash 2001) are plotted. We see that large radius (stiff at nuclear density) EOS are preferred. Formally, the relativistic field theoretical model by Müller & Serot (1996) and the model GS2 by Glendenning & Schaffner-Bielich (1999) are the only modern models allowed (the original PS model of Pandharipande & Smith (1975) is also allowed). We note that the GS models are very sensitive to the K meson potential; for example, GS1 is strongly excluded. Interestingly, no potential or variational method computations agree with the formal overlap. If one includes the distance uncertainty, a few more intermediate radius models are not excluded at the 90% CL. However, even including the distance uncertainties, all quark star models are excluded at the $\sim 95\%$ level for $M_{\text{NS}} \lesssim 1.5M_{\odot}$ and are only barely consistent at the highest allowed masses. Improved *HST* parallax measurements could boost this exclusion to the 3σ level.

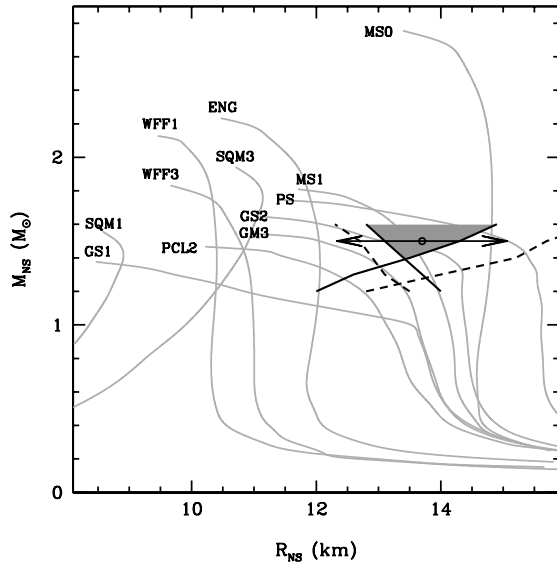


FIG. 5.— Radius constraints for different possible RX J1856–3754 masses. The triangular gray shaded region represents the formal 90% CL overlap from the pulse fraction and spectral constraints. The two-sided arrow represents the systematic range induced by the distance uncertainties. Equation of state curves and labels are drawn from Lattimer & Prakash (2001). See this paper for EOS labels and references.

The model GS2 differs from the MS models in that it includes a kaon condensate in the core. One principal effect of exotic interior condensates is to enhance neutrino cooling after ~ 100 y. This can also be achieved without exotica for a proton fraction $\gtrsim 11\%$ through the direct URCA process (Lattimer *et al.* 1991). Our inferred T_{cold} , interpreted as the signature of the cooling from the initial heat of formation, corresponds to $L \approx 3.2 \times 10^{31}$ erg/s for our best fit radius. Such luminosities are reached in $\sim 5 \times 10^5$ y (the preferred age of Walter & Lattimer 2002) when enhanced neutrino cooling can occur, but are achieved after $\sim 1.3 \times 10^6$ y for stars with low density (stiff) cores Tsuruta *et al.* (2002). Thus, depending on the actual stellar age, this cool surface may be seen as weak evidence for an exotic composition and/or significant softening of the EOS at very high densities.

The prospects for further tests of the ideas in this paper hinge on the detection of a pulse from RX J1856 – 3754 along with measurement of the pulse fraction and the period derivative. Given that significant allowed pulse fraction parameter space lies just slightly below the *CXO* LETG detection threshold, the prospects for a pulse measurement with the recently completed 58 ks *XMM* observation are quite good. Even if only thermal, the phase resolved spectrum should provide important constraints on the cap temperature, size and orientation. In particular our thermal model predicts that the pulse fraction should increase by 70% from 0.15 keV to 0.5 keV, where the *XMM* data should still deliver ~ 0.8 PN camera cps, allowing detection of pulse fractions well under 1%.

We are grateful to Boris Gänsicke for collaboration on the atmosphere models used in §2; and to Herman Marshall for sharing an independent LETG response matrix. This work was supported in part by NASA grant SP2-2002X.

REFERENCES

- Braje, T.M., Romani, R.W., & Rauch, K.P. 2000, *ApJ*, 531, 447
 Brazier, K. T. S. & Johnston, S. 1999, *MNRAS*, 305, 671
 Burwitz, V., Zavlin, V. E., Neuhäuser, R., Predehl, P., Trümper, & Brinkman, A. C. 2001, *A&A*, 379, L35
 Drake, J. J., Marshall, H. L., Dreizler, S., Freeman, P. E., Fruscione, A., Juda, M., Kashyap, V., Nicastro, F., Pease, D. O., Wargelin, B. J., & Werner, K. 2002 *ApJ*, 572, 996
 Gänsicke, B.T. Braje, T.M. & Romani, R.W. 2002, *A&A*, 386, 1001
 Glendenning, N. K. & Schaffner-Bielich, J. 1999, *Phys. Rev. C*, 60, 025803
 Greenstein, G. & Hartke, G. J. 1983, *ApJ*, 271, 283
 Harding, A. K. & Muslimov, A. G. 1998, *ApJ*, 508, 328
 Kaplan, D. L., van Kerkwijk, M. H., & Anderson, J. 2002, *ApJ*, 571, 447
 Lai, D. & Salpeter, E. E. 1997, *ApJ*, 491, 270
 Lattimer, J. M., Pethick, C. J., Prakash, M., & Haensel, P. 1991, *Phys. Rev. Lett.*, 66, 2701
 Lattimer, J. M. & Prakash, M. 2001, *ApJ*, 550, 426
 Müller, H. & Serot, B. D. 1996, *Nucl. Phys. A*, 606, 508
 Pandharipande, V. R. & Smith, R. A. 1975, *Nucl. Phys. A*, 237, 507
 Pavlov, G.G., Shibano, Y.A., Zavlin, V.E., & Meyer, R.D. 1995, in *The Lives of Neutron Stars*, ed. M. A. Alpar, Ü. Kiziloglu, & J. van Paradijs (Dordrecht: Kluwer), 71-90
 Pavlov, G. G., Zavlin, V. E., Trümper, J., & Neuhäuser, R. 1996, *ApJ*, 472, L33
 Pons, J. A., Walter, F. M., Lattimer, J. M., Prakash, M., Neuhäuser, R., & An, P. 2002, *ApJ*, 564, 981
 Rajagopal, M., Romani, R. W., & Miller, M. C. 1997, *ApJ*, 479, 347
 Rankin, J. M. 1993, *ApJ*, 405, 285
 Ransom, S. M., Gaensler, B. M., & Slane, P. O. 2002, *ApJ*, 570, L75
 Tsuruta, S., Teter, M.A., Takatsuka, T., Tatsumi, T. & Tamagaki, R. 2002, *ApJ*, 571, L143
 van Kerkwijk, M. H. & Kulkarni, S. R. 2001, *A&A*, 378, 986
 van Kerkwijk, M. H. & Kulkarni, S. R. 2001, *A&A*, 380, 221
 van Kerkwijk, M. H. 2002, *Proc. Jan van Paradijs Memorial Symposium*, ed. Van den Heuvel, E. P. J., Kaer, L., Rol, E., ASP, San Francisco
 Walter, F. M., Wolk, S. J., & Neuhäuser, R. 1996, *Nature*, 379, 233

Walter, F. M. 2001, ApJ, 549, 433

Walter, F. M. & Lattimer, J. 2002, astro-ph/0204199

Wang, F.Y-H., Ruderman, M., Halpern, J. P. & Zhu, T. 1998, ApJ,

498, 373

TABLE 1
PULSE FRACTION 90%/99% CONFIDENCE LIMITS

M_{NS} (M_{\odot})	No Prior (km)	$\Theta_{\text{rad}} = 10.6^{\circ}$ (km)	$\Theta_{\text{rad}} = 21.2^{\circ}$ (km)
1.2	10.3/14.6	11.3/15.6	12.0/16.3
1.3	10.5/16.7	11.7/17.6	12.6/19.2
1.4	12.2/17.8	13.1/18.9	13.6/19.9
1.5	13.4/19.4	13.8/21.0	14.3/21.3
1.6	14.0/20.0	14.6/21.4	14.9/21.2